Osteoarthritis and Cartilage 27 (2019) 1219–1228

Osteoarthritis and Cartilage

Evaluation of equine articular cartilage degeneration after mechanical impact injury using cationic contrast-enhanced computed tomography

B.B. Nelson †, J.T.A. Mäkelä ‡ §, T.B. Lawson ‡ ||, A.N. Patwa § ¶, M.F. Barrett #, C.W. McIlwraith †, M.B. Hurtig ††, B.D. Snyder ‡, V.J. Moorman †, M.W. Grinstaff § || ‡‡, L.R. Goodrich †, C.E. Kawcak † *

† *Equine Orthopaedic Research Center, Colorado State University, Fort Collins, CO, USA*
‡ *Center for Advanced Orthopaedic Studies, Beth Israel Deaconess Medical Center and Harvard Medical School, Boston, MA, USA*
§ *Department of Chemistry, Boston University, Boston, MA, USA*
|| *Department of Mechanical Engineering, Boston University, Boston, MA, USA*
¶ *SLSE (Chemistry), Navrachana University, Vadodara, Gujarat, India*
# *Department of Environmental and Radiological Health Sciences, Colorado State University, Fort Collins, CO, USA*
†† *Department of Clinical Studies, University of Guelph, Ontario, Canada*
‡‡ *Departments of Biomedical Engineering, and Medicine, Boston University, Boston, MA, USA*

ARTICLE INFO

Article history:
Received 13 December 2018
Accepted 16 April 2019

Keywords:
Cartilage imaging
Histology
Glycosaminoglycan
Biochemical
Osteoarthritis
Post traumatic OA

SUMMARY

Objective: Cationic agent contrast-enhanced computed tomography (cationic CECT) characterizes articular cartilage *ex vivo*, however, its capacity to detect post-traumatic injury is unknown. The study objectives were to correlate cationic CECT attenuation with biochemical, mechanical and histological properties of cartilage and morphologic computed tomography (CT) measures of bone, and to determine the ability of cationic CECT to distinguish subtly damaged from normal cartilage in an *in vivo* equine model.

Design: Mechanical impact injury was initiated in equine femoropatellar joints *in vivo* to establish subtle cartilage degeneration with site-matched controls. Cationic CECT was performed *in vivo* (clinical) and postmortem (microCT). Articular cartilage was characterized by glycosaminoglycan (GAG) content, biochemical moduli and histological scores. Bone was characterized by volume density (BV/TV) and trabecular number (Tb.N.), thickness (Tb.Th.) and spacing (Tb.Sp.).

Results: Cationic CECT attenuation (microCT) of cartilage correlated with GAG ($r = 0.74$, $P < 0.0001$), compressive modulus (E_{eq}) ($r = 0.79$, $P < 0.0001$) and safranin-O histological score ($r = -0.66$, $P < 0.0001$) of cartilage, and correlated with BV/TV ($r = 0.37$, $P = 0.0005$), Tb.N. ($r = 0.39$, $P = 0.0003$), Tb.Th. ($r = 0.28$, $P = 0.0095$) and Tb.Sp. ($r = -0.44$, $P < 0.0001$) of bone. Mean [95% CI] cationic CECT attenuation at the impact site (2215 [1987, 2443] Hounsfield Units [HUs]) was lower than site-matched controls (2836 [2490, 3182] HUs, $P = 0.036$). Clinical cationic CECT attenuation correlated with GAG ($r = 0.23$, $P = 0.049$), E_{eq} ($r = 0.26$, $P = 0.025$) and safranin-O histology score ($r = -0.32$, $P = 0.0046$).

Conclusions: Cationic CECT (microCT) reflects articular cartilage properties enabling segregation of subtly degenerated from healthy tissue and also reflects bone morphometric properties on CT. Cationic CECT is capable of characterizing articular cartilage in clinical scanners.

Introduction

Articular cartilage injury is a well-recognized and costly health care problem in both humans and horses[1,2]. Characterized by glycosaminoglycan (GAG) loss in the extracellular matrix (ECM), articular cartilage degeneration causes reduced water retention

* Address correspondence and reprint requests to: C.E. Kawcak, 300 W. Drake Road, Equine Orthopaedic Research Center, College of Veterinary Medicine and Biomedical Sciences, Colorado State University, Fort Collins, CO, 80523, USA.
E-mail address: ckawcak@colostate.edu (C.E. Kawcak).

https://doi.org/10.1016/j.joca.2019.04.015
1063-4584/

and compressive stiffness thereby promoting progressive deterioration[3,4]. Similarities in articular cartilage anatomy and physiology along with the challenges of detecting and treating early degeneration have established horses as a practical translational research model for humans[2,5].

Early detection of articular cartilage injury is critical to successful therapeutic strategies as this tissue has limited repair potential. Unfortunately, commonly used imaging techniques are incapable of providing this information. Magnetic resonance imaging (MRI) is a standard method used for articular cartilage evaluation but routine techniques only capture morphologic alterations that occur late in the disease process[6]. Quantitative MRI techniques (dGEMRIC, T1rho, T2 mapping) expand diagnostic sensitivity by providing biochemical evaluation[7]. Nevertheless, their use is commonly restricted to research institutions owing to their specialized equipment and software required, prolonged scan times and expertise needed for interpretation of the acquisition data. Multi-slice computed tomography (CT) is a widely available imaging method capable of volumetric joint evaluation with decreased costs and scan times, and higher spatial resolution compared to MRI[8].

Contrast agents are administered to outline articular structures on CT: denoted as CT arthrography or contrast-enhanced CT (CECT). Once in the joint space, commercially available anionic iodinated contrast media exhibit limited diffusion into articular cartilage because it is repelled by the highly negative charges from GAGs[3,9]. Conversely, recently developed cationic contrast agents are positively charged and electrostatically attracted to GAGs[9]. As such, the measured cationic CECT attenuation from articular cartilage is directly proportional to GAG concentrations providing a more sensitive technique than when using anionic contrast media[3,9,10]. Cationic CECT imaging *ex vivo* has been validated in bovine, murine, rabbit, equine and human articular cartilage explants[10–17]. Despite *ex vivo* success, the use of cationic CECT to characterize subtly damaged equine articular cartilage *in vivo* corresponding to early stage osteoarthritis has not been investigated.

The objectives of this study were to determine the ability of cationic CECT to distinguish subtly damaged from normal articular cartilage using an *in vivo* equine impact model and also to determine its capability as an *in vivo* diagnostic method. We hypothesized that cationic CECT attenuation distinguishes subtly damaged from normal articular cartilage and also reflects the biochemical, mechanical and histological attributes of the tissue. Furthermore, we hypothesized that cationic CECT will be successfully implemented *in vivo* and correlates with articular cartilage quality.

Materials and methods

Optimization of impactor device

A spring-loaded impact device with 6.45 mm diameter plane-ended tip was used to initiate subtle articular cartilage injury[18–20]. Device optimization was used to characterize impact force, stress, and energy variation, and establish the optimal force needed to extend cartilage injury into the transitional zone while preventing macroscopic surface disruption. Impact stresses were derived from a calibrated piezoelectric force transducer (Model 218C, PCB Piezotronics, Depew, NY) secured between the impactor shaft and tip while connected to a charge amplifier (Model 421A11, PCB Piezotronics)[20]. Impact stress from the transducer signal (48 kHz) was calculated by normalizing peak force to the cross-sectional area of the impactor tip (32.7 mm^2)[20]. To calibrate the system, the femoral trochlea from a 3-year-old female horse weighing 440 kg (euthanized for reasons unrelated to this study) was collected with no articular cartilage lesions and tested within 1 h of sacrifice. Six different impact forces were delivered (six replicates per impact) across the surface, maintaining a consistent impact duration. After impact, articular cartilage was examined macroscopically and for cell viability distributions (LIVE/DEAD Viability/Cytotoxicity, Life Technologies™, Grand Island, NY)[21]. Mixtures of calcein acetomethoxyester (1:2000) and ethidium homodimer (1:3000) in 1X PBS were added to articular cartilage samples, incubated for 1 h at 20°C and examined under a fluorescence microscope equipped with a digital camera (QImaging, MicroPublisher, 5.0 RTC, Surrey, Canada) to characterize depth of injury and regional chondrocyte death following impact.

In vivo delivery of articular cartilage impacts

Four skeletally mature horses (aged 2–4 years; two females, two castrated males; weighing 375–460 kg) with no lameness, femoropatellar joint effusion or radiographic abnormalities were used (Animal Care and Use Committee Protocol 14–4924A). Lameness examinations and assessments of femoropatellar joint effusion[5] were performed.

Clinical cationic CECT acquisition

The CA4+ contrast medium was prepared at 24 mg I/mL (400 mOsmol/kg, pH = 7.4)[9]. Before inducing articular cartilage injury, a baseline clinical cationic CECT examination was performed on both femoropatellar joints[8]. Synovial fluid was collected aseptically for cytologic and biochemical analysis followed by injection of 100 mLs of CA4+. Clinical cationic CECT examinations (Gemini Big Bore, Philips Healthcare, Andover, MA) were performed 4 h later under general anesthesia with a density phantom. Preliminary *in vivo* experimentation indicated 4 h after injection provided optimal diffusion into femoropatellar cartilage[22]. Parameters of all CT acquisitions (Supplementary Item 1) facilitated in-plane resolution of 0.292 × 0.292 mm by 0.8 mm thickness. At 70 days after impact, the clinical cationic CECT examinations were repeated.

Arthroscopic procedure to impact articular cartilage

Following baseline clinical cationic CECT examination, both joints were prepared for arthroscopic surgery. One stifle in each horse was randomly assigned (block randomization) to receive the impacted defects while the contralateral limb was sham-operated. The femoral trochlea was used due to its common use in equine cartilage repair studies and to maximize arthroscopically accessible cartilage surface area compared to the femoral condyle[2,5]. The impactor tip contacted the medial trochlear ridge of the femur (Fig. 1) through an arthroscopic portal in both impact and control joints. Nine, 41 MPa force impacts were delivered in a diamond pattern creating a 19.35 mm diameter impact region (impact joints only). The impactor tip was applied to the same site in control joints but was not activated. The boundary of the impact site in impact and control joints was marked using an 18-gauge needle identifiable at sacrifice. After surgery, the horse was maintained on stall confinement until incisional healing (12 days) and then permitted free exercise[2].

Clinical and synovial fluid assessments

After baseline at 2-week increments, lameness examinations and joint effusion assessments were repeated by the same blinded investigator, and synovial fluid aspirates were collected and analyzed for leukocyte counts (hematology analyzer), total protein (refractometry) and a separate aliquot stored at −80°C for biochemical analysis. Biochemical analyses included determination of GAG using the 1,9-dimethylmethylene blue (DMMB) assay and prostaglandin E_2 (PGE_2) concentrations (Enzo Life Sciences, Inc. Farmingdale, NY)[4,23]. DMMB samples were run in triplicate,

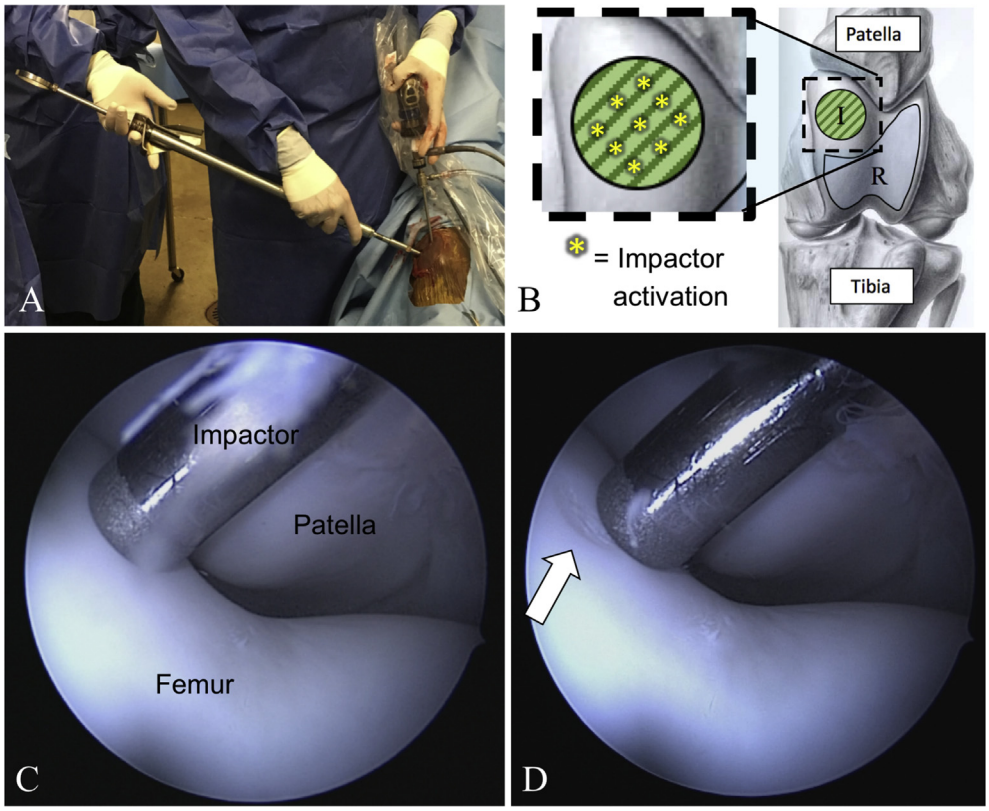

Fig. 1. Operative images showing the impact device being used *in vivo* (Image A). Image B identifies the segregation of sites (I, impact; R, remote) in both impact and control joints, and shows the distribution of impacts delivered within the impact site. Arthroscopic images showing placement of the impactor on the medial trochlear ridge of the femur before (image C) and after (image D) impact. Note the subtle contusion delivered to the medial trochlear cartilage (arrow).

compared to known concentrations of chondroitin sulfate (C6737, Sigma–Aldrich, St. Louis, MO) and read at 530 nm on a microplate reader (SpectraMax M3, Molecular Devices, Sunnyvale, CA). PGE_2 samples were extracted with C2 columns (Amprep mini-columns, GE Healthcare, Pittsburgh, PA), run in duplicate and read at 405 nm.[4]

Postmortem assessments

After 70-day clinical cationic CECT examinations, horses were euthanized (pentobarbital 39 mg/kg IV), and the stifles removed. Postmortem MRI examinations (1.5 T, Signa 9.1, GE Healthcare, Waukesha, WI) were performed immediately post sacrifice using proton density (with and without fat suppression), T2-weighted, and T1-weighted fast spin echo and spoiled gradient recalled echo sequences (Supplementary Item 1) and then frozen at −20°C until further evaluation.

Samples from each stifle underwent all mechanical testing and microCT imaging assessments after thawing[24,25]. Synovial membrane biopsies were collected and stored in 10% formalin. Under irrigation, ten osteochondral plug biopsies (7 mm diameter, >1 cm of subchondral bone) were collected along the medial (5 plugs) and lateral (5 plugs) trochlear ridge surfaces using a diamond tipped cylindrical coring drill bit (Starlite Industries, Bryn Mawr, PA). Each osteochondral biopsy was scored using the International Cartilage Repair Society (ICRS)[26] system followed by equilibration overnight in a preservative solution (5 mM Benzamidine HCl, 5 mM EDTA, Sigma–Aldrich; 1xAntibiotic-Antimycotic, Life Tech, Carlsbad, CA) to remove residual CA4+[15].

Mechanical testing

After saline equilibration, articular cartilage thickness of each osteochondral biopsy was determined with microCT (μCT40, ScancoMedical, Brüttisellen, Switzerland) at 70 kVp, 113 μA, 300 ms integration time and 36-μm isotropic voxel resolution. Imaging data were imported into Analyze software (AnalyzeDirect, Overland Park, KS). Articular cartilage volume object maps were created using a semi-automatic threshold-based algorithm and sampled at 400 locations to generate an average thickness. Each plug was rigidly clamped in a mechanical testing apparatus (Enduratec3230, BOSE, Eden Prairie MN) and a stress-relaxation protocol in unconfined geometry applied to the articular surface using a nonporous ultrahigh molecular weight polyethylene platen while immersed in 400 mOsm/kg saline solution. The stress-relaxation regimen consisted of four incremental 5% compressive strain steps (0.333% thickness/sec) with a 45-min relaxation period between steps collected at 10 Hz. A linear fit to stress vs strain at equilibrium was used to calculate compressive Young's modulus (E_{eq}). The dynamic response was calculated separately at each displacement step and reported as Equilibrium (E_{dyn}) and strain-dependent ($E\varepsilon$) dynamic modulus[27]. To estimate tissue permeability, stress-relaxation time (τ) and stretching parameter (β) constants were calculated[28] using MATLAB (R2017a, Mathworks, Natick, MA).

Cationic CECT (microCT)

After mechanical testing, all osteochondral plugs were immersed in CA4+ (24 mg I/mL, ~20X cartilage volume) for 24 h at 20°C (to ensure equilibrium) and then re-imaged with microCT[13,15]. A semi-automatic threshold-based segmentation procedure (0–4500 Hounsfield units [HUs]) was performed with manual correction to ensure accuracy. Cationic CECT attenuation of cartilage was converted into HUs using a concurrently scanned deionized water sample.

Osteochondral plugs were then equilibrated overnight in preservative solution to remove residual CA4+. The full thickness

cartilage from each biopsy was bisected and removed with a scalpel blade. One portion was frozen at −80°C for biochemical analysis, while the remaining osteochondral portion was fixed in 10% formalin for histologic analysis.

Bone morphometric analysis

Bone morphometry calculations were performed using commercial software (ScancoMedical, Brüttisellen, Switzerland). A cylindrical (59.36 mm^3) region-of-interest (ROI) was generated in the subchondral trabecular bone of each plug using an automated threshold algorithm (467–3,000 mg HA/cm^3). Trabecular parameters were reported as bone volume fraction (BV/TV), trabecular number (Tb.N.), thickness (Tb.Th.), and separation (Tb.Sp.); and bone mineral (BMD) and tissue mineral (TMD) density using the direct 3D method[11]. The subchondral bone plate was segmented, and the thickness determined as described for cartilage.

Biochemical and histological analyses

Articular cartilage allocated to biochemical evaluation was weighed (wet weight), lyophilized for 24 h, re-weighed (dry weight), and papain digested (1 mg/mL, P4762, Sigma–Aldrich) to quantify GAG and total collagen (DMMB and hydroxyprolines assays, respectively)[29]. DMMB samples were run as above and reported as % wet weight. Hydroxyproline samples were hydrolyzed with 12.1N HCl at 110°C for 16 h, mixed with 50 mM chloramine T (402869, Sigma–Aldrich) at 20°C for 20 min, and then mixed with 1M 4-dimethyl-aminobenzaldehyde (156477, Sigma–Aldrich). Samples were plated in duplicate, read at 550 nm, converted to known hydroxyproline concentrations, and reported as % dry weight (H54409, Sigma–Aldrich).

Histologic evaluation

After osteochondral samples were decalcified (Formical-2000, McKinney, TX), all histologic samples were embedded in paraffin and 5-μm section microscope slides prepared. All tissues were stained with hematoxylin and eosin. Osteochondral samples were additionally stained with safranin-O fast green (SOFG). Bovine trachea and equine osteochondral tissues were included to ensure consistent staining across batches.

Histologic scoring

The Osteoarthritis Research Society International (OARSI) scoring system was used by a blinded observer to grade synovial membrane and articular cartilage[30]. Articular cartilage was scored for chondrocyte necrosis, chondrone (cluster) formation, cartilage fibrillation/fissuring, focal cell loss and global SOFG uptake. Subchondral bone was scored for osteochondral lesions, remodeling and splitting. Ranges for cumulative scores were 0–20 (cartilage), 0–10 (bone), and 0–30 (OARSI). Articular cartilage sections were also individually scored for safranin-O uptake in tangential, transitional, and radiate (territorial and interterritorial) zones defined as 10%, 50%, and 40% of mean cartilage thickness, respectively, and a cumulative score was determined (range 0–16).

Clinical cationic CECT evaluation

Following osteochondral biopsy removal, the cored femoral trochlea was imaged with CT (Pegaso, Epica Medical Innovations, San Clemente, CA) providing a template for accurate comparisons of plug data (microCT, biochemical, mechanical and histological) to clinical imaging (cationic CECT and MRI). The CT settings (Supplementary Item 1) permitted isotropic voxel dimensions of 0.3 mm^3. Using the 3-D voxel registration module (Analyze®), the post-coring mask from each joint was manually aligned over each clinical imaging scan. Segmented ROIs of articular cartilage were generated from the axial slices and manually verified to ensure the captured volume only included cartilage. After density phantom correction, CECT attenuation was reported in HUs.

MRI evaluation

The post-coring mask was also co-registered with the MRI images. A board-certified radiologist blinded to group allocation performed all scoring[31]. Articular cartilage at each site was scored for cartilage volume/fill, and for T2 and T1 signal intensity. Subchondral bone signal intensity was scored on the PD with fat saturation (PDFS) sequence.

Data and statistical analysis

Categorical data were reported as median ± interquartile (IQR) range and continuous data as mean ± 95% confidence intervals [lower limit, upper limit]. Data from osteochondral biopsies ($N = 80$, experimental unit) were analyzed between impact and control joints from the four horses. Two articular cartilage sites (impacted and remote) were categorized within each impact and control joint [Fig. 1(B)]. The impacted site defined the location of the delivered contusion in the impact joint, while it was a regionally-specific control in the control joint, addressing the inherent variability that occurs across the articular surface[32,33]. Correlation between variables was calculated accounting for repeated measures on subjects[34] and correlation strength was characterized[35].

Articular cartilage, bone morphometry and clinical CECT measures were analyzed using mixed model analysis. Fixed effects included joint (impact or control), site (impact or remote) and joint*site interaction. Horse and horse*joint were included as random effects to account for repeated measures. Serially acquired continuous data (e.g., synovial fluid assessments) were also compared using mixed-effects models. Fixed effects included joint and time point. Horse and horse*joint were included as random effects. Assumptions of each mixed model analysis were assessed based on visual inspection of residual diagnostic plots. Categorical data were compared using a Wilcoxon signed rank test.

Histological data were compared to imaging parameters after establishing a threshold of injury determined by receiver operator characteristic (ROC) curve analysis. Histological scores were identified based on their anatomic location at the impacted site and confirmed to decline in GAG and E_{eq} compared with control joint cartilage. Using the ROC curve, the maximum Youden index established a threshold of impacted articular cartilage damage on the OARSI scale. Statistical analyses were performed using SAS (SAS University Edition, v9.2, SAS Institute Inc., Cary, NC) and significance defined as $P < 0.05$.

Results

Optimization of impactor device

A 41 (±2.8) MPa impact consistently induced articular cartilage injury extending into the transitional zone, while preventing macroscopic surface disruption. The 52 (±1.3) and 71 (±5.7) MPa impacts all induced a palpable defect, while lower impact forces did not cause macroscopically visible or palpable defects in the articular surface. Microscopic evaluation and chondrocyte viability staining showed a proportional increase in the depth of cartilage injury with impact force (Supplementary Item 2).

In vivo delivery of articular cartilage impacts

Macroscopic inspection of articular cartilage at 70 days post-impact revealed minor surface bruising, blistering and palpable fibrillation (ICRS scores 1 (1–1)), while there was a normal

confluent surface to the remote regions in the impact joint and in all control joint surfaces (ICRS scores 0 (0–0)). No other evidence of joint disease was detected. A difference between impact (1 [0.75–1.25]) and control (1.5 [1–2]) joints in cumulative synovial membrane score was not detected (Supplementary Item 3). Differences between impact and control joints were not detected for any synovial fluid, lameness, or synovial effusion assessments.

The impact site cartilage from impacted joints had lower cationic CECT attenuation reflecting similar distributions of safranin-O stain uptake compared to control joints (Fig. 2). Cationic CECT attenuation (microCT) strongly correlated with GAG ($r = 0.74$, $P < 0.0001$), E_{eq} ($r = 0.79$, $P < 0.0001$) and tissue permeability (τ: $r = 0.59$, $P < 0.0001$; β: $r = 0.59$, $P < 0.0001$) (Fig. 3(A)–(C), Table I). Mean cationic CECT attenuation at the impacted site (2215 [1987, 2443] HUs) was significantly lower than the remote sites in impact joints (2783 [2589, 2977] HUs, $P < 0.0001$) and when compared to the same site in control joints (2836 [2490, 3182] HUs, $P = 0.036$) [Fig. 3(C)]. Cationic CECT attenuation (microCT) strongly correlated with the cumulative region SOFG score ($r = -0.66$, $P < 0.0001$) and cumulative OARSI histology score ($r = -0.61$, $P < 0.0001$) [Fig. 4(A) and (B)]. At the impact site, there were significantly higher SOFG scores in impact joints compared to control joints [Fig. 4(C)]. Cationic CECT attenuation decreased as SOFG scores increased [Fig. 4(D)]. Cationic CECT attenuation (microCT) was significantly correlated with most individual OARSI scoring components and cumulative scores (Table II). The ROC curve analysis established a maximum Youden index of 9 (98.6% sensitivity, 100% specificity, area under the curve = 0.9932) to define impacted from remote articular cartilage [Fig. 5(A)]. Using this threshold, cationic CECT attenuation was significantly lower in OARSI scores ≥9 (2249 [2060, 2437] HUs) compared to those <9 (2694 [2570, 2817] HUs, $P < 0.0001$) [Fig. 5(B)].

Cationic CECT attenuation of cartilage significantly correlated with BV/TV ($r = 0.37$, $P < 0.0005$), Tb.N. ($r = 0.39$, $P = 0.0003$), Tb.Th. ($r = 0.28$, $P = 0.0098$) and Tb.Sp. ($r = -0.44$, $P < 0.0001$) of bone (Table I). Despite significant correlations with cationic CECT, differences in bone morphometry parameters were not detected between groups.

At the endpoint scans, clinical cationic CECT attenuation correlated with GAG ($r = 0.23$, $P = 0.049$), E_{eq} ($r = 0.26$, $P = 0.025$), cumulative SOFG score ($r = -0.32$, $P = 0.0046$) and cationic CECT (microCT) attenuation ($r = 0.43$, $P = 0.0001$) [Fig. 6(A)–(C)]. A difference in clinical cationic CECT attenuation between SOFG scores was not detected [Fig. 6(D)]. All individual zonal, cumulative and overall SOFG scores significantly correlated to clinical cationic CECT attenuation (Table II). A difference between impact and remote sites was not detected on MRI.

Discussion

Correlations between cationic CECT attenuation, obtained via microCT, and GAG and E_{eq} are reported for normal and enzymatically degenerated articular cartilage *ex vivo*[10–14,36]. This study, however, reveals that these findings apply to mechanically induced injury *in vivo*, which more closely represents natural post-traumatic osteoarthritis etiology than enzymatically induced degradation. Cationic CECT attenuation distinguishes subtly damaged from normal articular cartilage reflecting the altered biochemical, mechanical and histologic properties of the tissue, supporting our hypothesis.

Most individual and all cumulative OARSI histologic scoring components of cartilage correlate to cationic CECT attenuation (microCT). Moreover, the ROC analysis establishes a highly sensitive and specific threshold of injury; samples reaching the threshold exhibit lower cationic CECT attenuation than samples that do not. While cationic CECT does not directly measure certain individual OARSI scoring components (e.g., chondrocyte necrosis), those components are not mutually exclusive occurring concurrently with GAG depletion in degenerative articular cartilage[30]. Thus, the apparent connection between cationic CECT and scoring components indirectly associated with GAG reflect the collinearity of histologic parameters in the scoring system. Correlations between cationic CECT attenuation and SOFG histologic scores are explained by the similar electrostatic mechanism of action of each respective technique. Both CA4+ and safranin-O are cationic compounds that bind proportionally to the negatively charged GAGs in the ECM and are quantified with CT imaging and microscopy, respectively[37]. As such, cationic CECT attenuation reflects the same GAG distributions as histology albeit non-destructively. Furthermore, cationic CECT characterizes GAG distribution in a tissue volume compared to histology, which is limited by the number of individual sample slices processed[37]. Though synovial membrane histologic scores

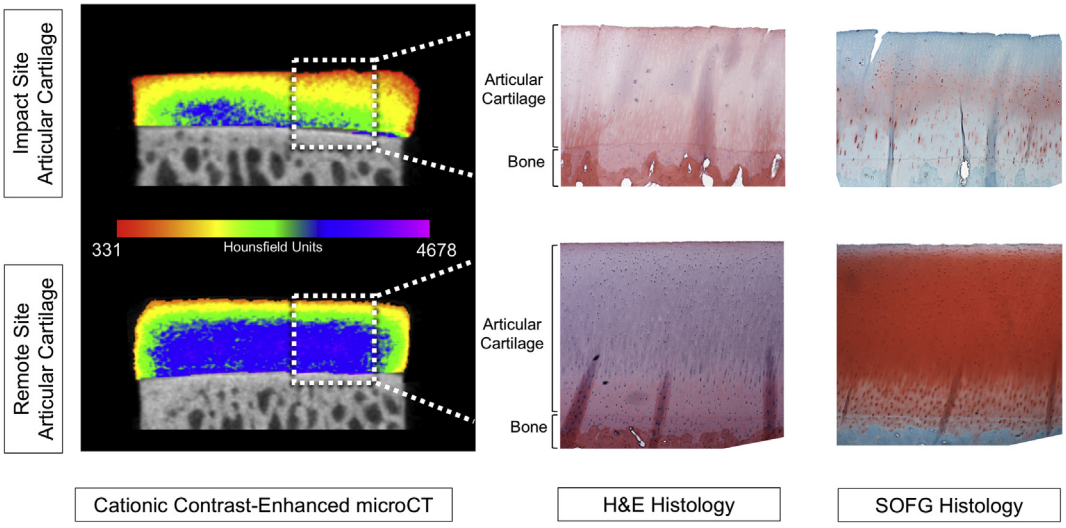

Fig. 2. Representative cationic contrast-enhanced computed tomography (CECT) (microCT) images of equine articular cartilage 70 days after impact injury compared with remote cartilage in an impact joint. A color map highlights the changes in distribution of cationic contrast medium (CA4+) uptake in articular cartilage. Histological images are stained with hematoxylin and eosin (H&E) and safranin-O fast green (SOFG). Note the similar distribution of CA4+ and safranin-O stain uptake within samples: low cationic CECT attenuation corresponds to low safranin-O.

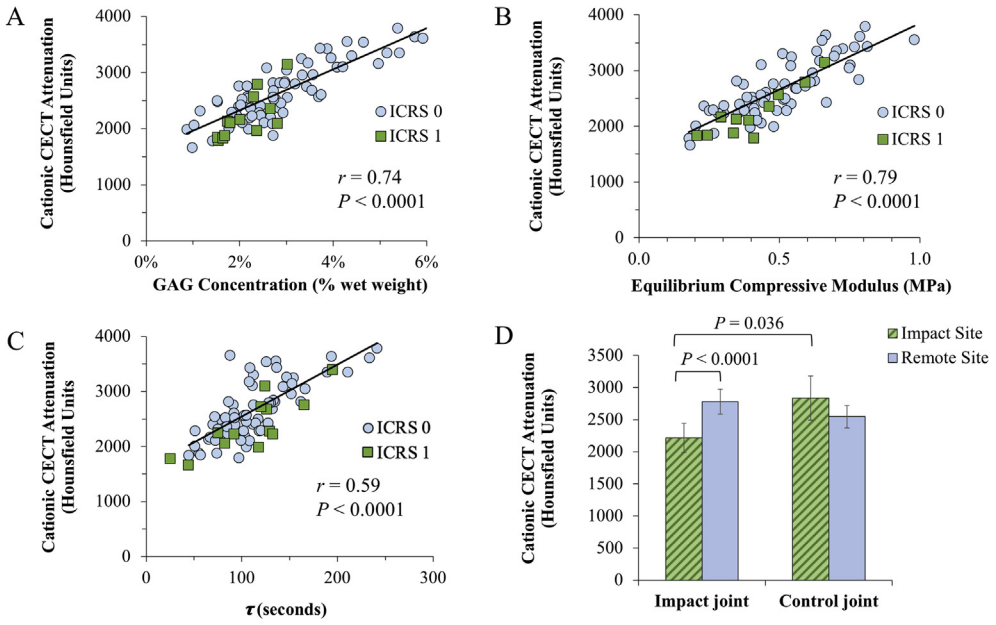

Fig. 3. Comparison of cationic contrast-enhanced computed tomography (CECT) (microCT) with glycosaminoglycan (GAG) concentration (image A), equilibrium compressive modulus (image B) and permeability (τ, image C). Data points in each image are additionally identified by their macroscopic scoring on the International Cartilage Repair Society (ICRS) scale. Correlation coefficients (r) and P-values identify the strength of correlation between variables using a Bland correlation controlling for repeated measures between subjects. Mean cationic CECT attenuation at the impacted and remote cartilage sites within the impact and control joints are shown in image D (error bars: 95% confidence interval).

Table I
Correlations between cationic CECT attenuation (microCT) and GAG with biochemical, mechanical and bone parameters. Correlation coefficients (r) and P-values identify the strength of correlation between variables using a Bland correlation controlling for repeated measures between subjects.GAG, glycosaminoglycan; E_{eq}, equilibrium compressive Young's modulus; E_{dyn}, dynamic Young's modulus $E\varepsilon$, strain-dependent dynamic modulus; BV/TV, bone volume fraction; Tb.N., trabecular number; Tb.Th., trabecular thickness; Tb.Sp., trabecular spacing; BMD, bone mineral density; TMD, tissue mineral density; τ, stress-relaxation time constant; β, stretching parameter constant; N/A, not applicable

Parameter	Cationic CECT Attenuation		GAG Concentration	
	r	P-value	r	P-value
GAG concentration	0.74	<0.0001	N/A	N/A
E_{eq}	0.79	<0.0001	0.65	<0.0001
5% E_{dyn}	0.34	0.0025	0.20	0.092
10% E_{dyn}	0.16	0.184	0.14	0.254
15% E_{dyn}	0.16	0.158	0.16	0.181
20% E_{dyn}	0.17	0.148	0.17	0.147
E_{dyn}	0.30	0.009	0.12	0.3
$E\varepsilon$	0.02	0.83	0.11	0.35
T	0.59	<0.0001	0.62	<0.0001
B	0.59	<0.0001	0.62	<0.0001
Total collagen	−0.32	0.0031	−0.24	0.0293
BV/TV	0.37	0.0005	0.25	0.0227
Tb.N.	0.39	0.0003	0.32	0.0045
Tb.Th.	0.28	0.0095	0.23	0.0359
Tb.Sp.	−0.44	<0.0001	−0.34	0.0019
Trabecular bone BMD	0.20	0.069	0.15	0.198
Trabecular bone TMD	0.02	0.839	0.00	0.962
Subchondral plate thickness	0.35	0.0022	0.17	0.158
Subchondral bone density	0.40	0.0004	0.36	0.0020

were low and differences between impact and control joints were not detected, all joints were exposed to CA4+ and synovial membrane samples unexposed to CA4+ were not available for comparison. Despite the lack of observed toxicity, further investigation of long-term effects of CA4+ on joint tissues are needed.

Articular cartilage impact models replicate the contusive injury that initiates post traumatic osteoarthritis, though the impact force used to induce cartilage injury varies between studies[18,19,38–43]. Experimental studies in other species document that lower impact forces establish disease[43–46]. The optimization experiment showed that a 41-MPa impact initiates subtle degenerative changes in equine femoral trochlear cartilage extending into the transitional zone. Despite the successful creation of articular cartilage injury *in vivo*, fulminant disease is not established in the femoropatellar joint compartment as evidenced by the lack of changes in synovial fluid, lameness and synovial effusion parameters between the impacted and control joints that commonly occur with osteoarthritis[4,19,23,47,48]. A similarly designed equine study using this impactor device at a higher impact force and for a longer study duration resulted in more severe injury while establishing a broad spectrum of articular cartilage injury, including progression to osteoarthritis[19]. In this study, the short (70-day) duration examined postimpact in a low weight bearing compartment likely precluded the necessary time for fulminant joint disease to develop.

Osteoarthritis is a disease that affects both articular cartilage and bone and there is a synergistic exchange between these two tissues important for normal joint function[1,49]. The cationic CECT attenuation from articular cartilage also moderately correlates with morphologic CT-based features of subchondral and trabecular bone. Correlations between cationic CECT attenuation and bone morphometric properties are observed and similar to a human metacarpophalangeal joint cartilage study[11]. In concert with Lakin *et al.*[11], these results reinforce the knowledge that pathologic bone responses occur following articular cartilage injury and cationic CECT provides quantification of both articular cartilage and bone, enabling and hastening the concurrent evaluation of these two tissues.

The cationic CECT technique is successfully implemented in living horses. Correlations are observed between clinical cationic CECT attenuation and SOFG histologic scores, though they are less robust than correlations obtained with microCT. While the co-registration methods ensured accuracy in comparing osteochondral plug data to the clinical imaging data sets, the lower spatial and contrast resolution, number of voxels per region-of-interest, signal-

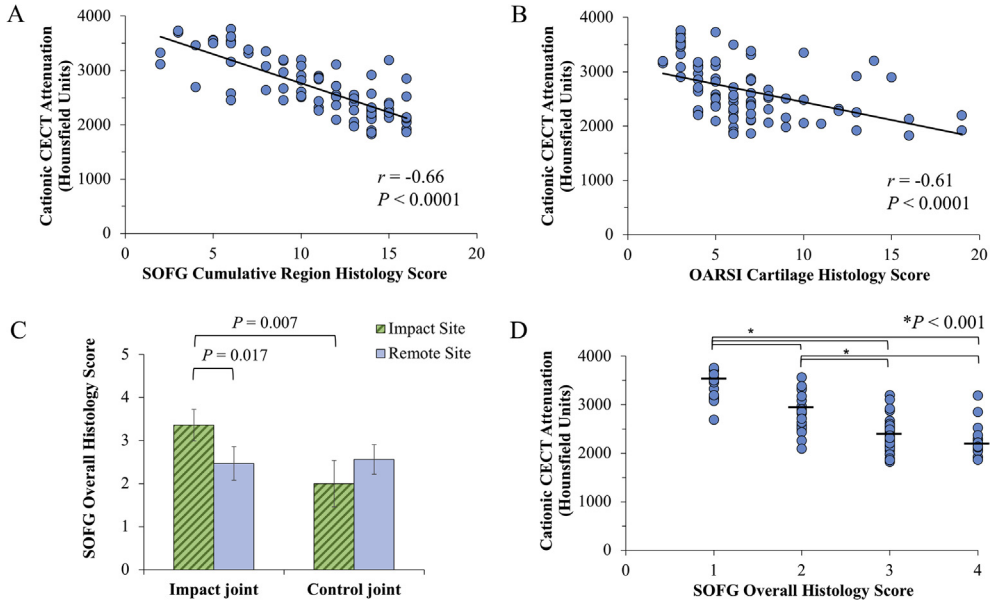

Fig. 4. Comparison of cationic contrast-enhanced computed tomography (CECT) (microCT) with safranin-O (SOFG) stain uptake cumulative score (image A) and the Osteoarthritis Research Society International (OARSI) cartilage score (image B). The SOFG cumulative score is a compilation of all sub-region (tangential, transitional, and radiate [territorial and interterritorial]) scores. The OARSI score incorporates chondrocyte necrosis, cluster formation, fibrillation/fissuring, focal cell loss and overall (global) SOFG uptake as well as osteochondral lesions, remodeling and osteochondral splitting of the attachments to subchondral bone. Correlation coefficients (r) and P-values identify the strength of correlation between variables using a Bland correlation controlling for repeated measures between subjects. Mean overall SOFG scores in the impacted and remote cartilage sites within the impact and control joints are shown in image C (error bars: 95% confidence interval) and mean cationic CECT attenuation value at each SOFG score are shown in image D.

Table II
Correlation coefficients (r) and P-valuesbetween histologic Osteoarthritis Research Society International (OARSI) parameters and cationic CECT attenuation (microCT and clinical scanner). Correlation between variables was performed using a strategy to control for repeated measures between subjects. SOFG, safranin-O fast green; OC, osteochondral; SCB, subchondral bone

Histologic parameter	*MicroCT*		*Clinical Scanner*	
	r	P-value	r	P-value
Chondrocyte necrosis	−0.65	<0.0001	−0.29	0.0106
Cluster formation	−0.33	0.0024	−0.15	0.199
Fibrillation fissuring	−0.35	0.0012	−0.19	0.093
Focal cell loss	−0.37	0.0006	−0.28	0.0156
SOFG overall	−0.67	<0.0001	−0.27	0.0178
Cumulative cartilage score	−0.62	<0.0001	−0.29	0.0103
SOFG tangential	−0.30	0.0062	−0.29	0.0117
SOFG transitional	−0.69	<0.0001	−0.26	0.0223
SOFG radiate territorial	−0.54	<0.0001	−0.20	0.0077
SOFG radiate interterritorial	−0.62	<0.0001	−0.31	0.0057
Cumulative SOFG score	−0.66	<0.0001	−0.32	0.0046
OC lesions	−0.18	0.096	−0.09	0.443
SCB remodeling	−0.17	0.132	−0.05	0.649
OC splitting	−0.13	0.249	−0.03	0.780
Cumulative bone score	−0.23	0.0034	−0.07	0.546
Cumulative OARSI score	−0.61	<0.0001	−0.24	0.0355

to-noise ratio, and range of attenuation values in clinical scanners compared to microCT likely cause these observed differences. Additionally, clinical imaging was performed in intact joints that have soft tissue densities influencing imaging resolution, whereas microCT was performed on osteochondral explants, and CA4+ diffusion rates *in vivo* differ from *ex vivo*[13,15,22]. The histological sections and GAG measurements are representative values while the cationic CECT measurements (microCT and clinical) are comprised of the entire plug volume. This partitioning of samples potentially affords variability between measurements. However, these correlation strengths are similar to other *ex vivo* studies that did not partition samples[10,12,13,50]. The quantity of analyses performed on each plug delayed biochemical and histological processing for 48–72 h. Despite detected correlations of these data with other outcomes and that differences over time were not detected using this methodology, earlier processing could alter these data. The negative correlation between clinical cationic CECT attenuation with SOFG staining is explained by the inverse relationship of these two measures. Increased SOFG scores are associated with lower matrix staining and therefore decreased GAG content. The decreased CA4+ binding to GAG then causes decreased cationic CECT attenuation. Despite correlations between clinical cationic CECT and histologic measures, differences between the control and impact joints were not found. Therefore, further investigations are required to determine if current clinical CT scanners possess sufficient resolution to distinguish subtle injury from healthy cartilage.

The MRI sequences did not distinguish healthy from impacted articular cartilage. While these morphologic sequences are routinely used in clinical practice, they are insensitive in documenting the early biochemical changes captured with quantitative methods (e.g., dGEMRIC, T1rho, T2 mapping). The MRI sequences were selected in order to confirm that the injury created was subtle enough to elude detection by current clinical standard imaging techniques. The lack of MRI signal quantification and use of subjective scoring (as opposed to quantification) was not suitable to directly compare the MRI data with clinical cationic CECT. The small number of horses used, and subtle injury inflicted by the impactor likely lessened detection rates by clinical scanners. Further directions of this work include comparing these cationic CECT results with quantitative MRI techniques and to determine how impacted cartilage can be distinguished from normal articular cartilage using quantitative MRI.

In conclusion, this impact model successfully creates subtle articular cartilage injury akin to early post-traumatic OA that is distinguished from normal articular cartilage using cationic CECT imaging in horses. The correlations of clinical cationic CECT to the biochemical, mechanical and histologic outcomes in horses are promising for this technique to extend into the clinic. However,

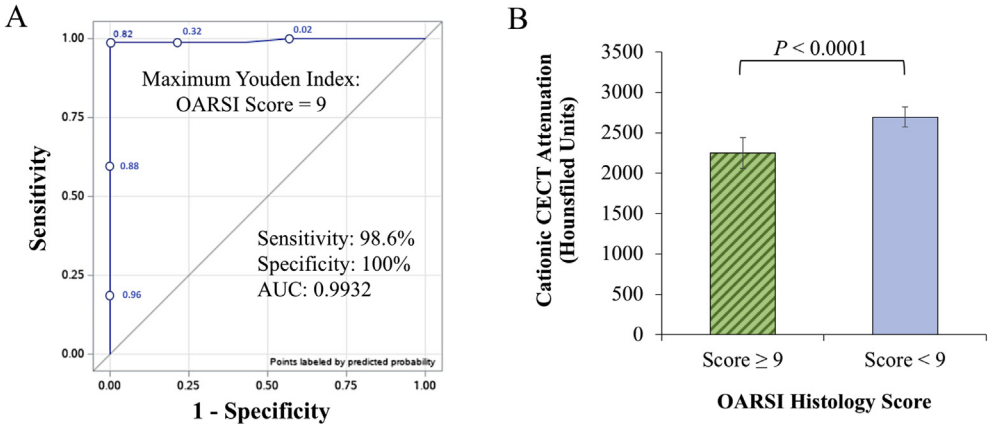

Fig. 5. Receiver operator characteristic (ROC) curve analysis demonstrating the threshold (maximum Youden index) of histological score to identify impacted cartilage (image A). Comparison of mean cationic CECT attenuation at cartilage samples above and below the ROC established threshold (image B) (error bars: 95% confidence interval). OARSI, osteoarthritis research society international; AUC, area under the curve.

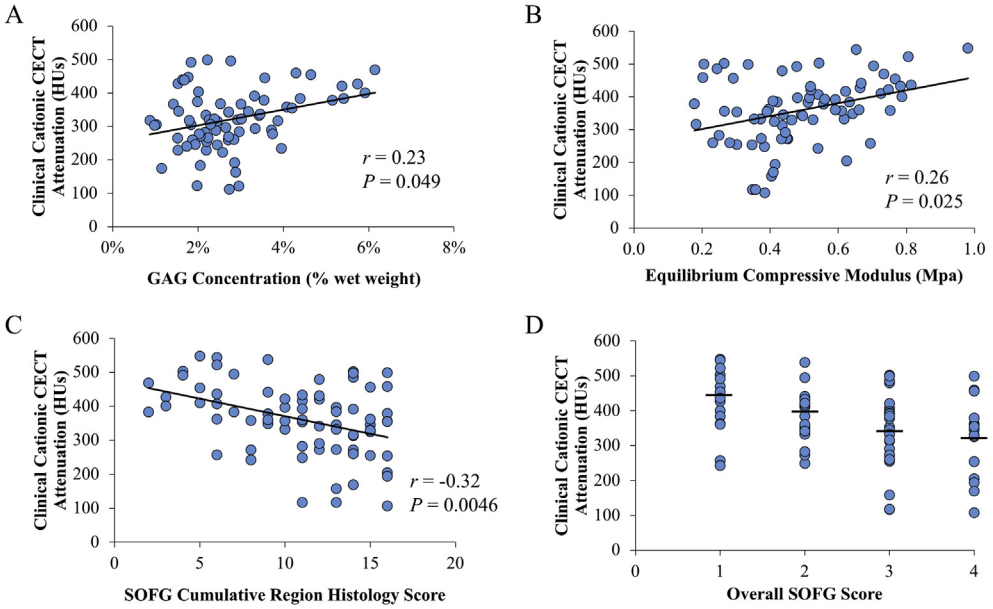

Fig. 6. Comparison of cationic contrast-enhanced computed tomography (CECT) acquired in a clinical scanner with glycosaminoglycan (GAG) content (image A), equilibrium compressive modulus (image B), safranin-O (SOFG) cumulative score (image C) and at each level of SOFG score (image D). Correlation coefficients (*r*) and *P*-values identify the strength of correlation between variables using a Bland correlation controlling for repeated measures between subjects.

these observed statistical correlations do not necessarily equate to clinical relevance, and the repeatability of these results, *in vivo* diffusion kinetics, safety, excretion profile, and ability to detect healing cartilage tissue require further investigation in horses and humans. Non-destructive imaging methods such as cationic CECT hold promise to detect early articular cartilage injury enabling the quantification and characterization of subtle articular cartilage injury with concurrent evaluation of bone.

Author contributions

B.B.N., M.W.G., C.W.M., M.B.H., L.R.G., and C.E.K. contributed to the conception and design of the study; B.B.N. conducted all experiments and organized all collected data. Experimental data was acquired by B.B.N., J.T.A.M., T.B.L., A.N.P., M.B.F., B.D.S. and V.J.M. Data analysis and interpretation was initiated by B.B.N. and reviewed by M.W.G., M.F.B., C.W.M., L.R.G. and C.E.K. All authors contributed to critical revision of the article and approval of the final version.

Conflict of interest

Authors have no conflict of interest to disclose.

Role of the funding source

Funding for the study was provided by the CVMBS Cooperative Veterinary Scientist Research Training Fellowship (Nelson) & College Research Council at Colorado State University , and the Finnish Cultural Foundation (Mäkelä). Study sponsors did not contribute to the study design, collection, analysis and interpretation of data; in the writing of the manuscript; or in the decision to submit the manuscript for publication.

Acknowledgments

The authors acknowledge the assistance of Jennifer Daniels, J. Nikki Phillips, and Equine Orthopaedic Research Center animal care staff; Dr Benjamin G. Cooper, Dr Kelly Zersen, Dr John D. Kisiday, Dan J. Brooks and Dr Ann Hess.

Supplementary data

Supplementary data to this article can be found online at https://doi.org/10.1016/j.joca.2019.04.015.

References

1. Brandt KD, Dieppe P, Radin E. Etiopathogenesis of osteoarthritis. Med Clin 2009;93:1–24.
2. McIlwraith CW, Fortier LA, Frisbie DD, Nixon AJ. Equine models of articular cartilage repair. Cartilage 2011;2:317–26.
3. Bansal PN, Joshi NS, Entezari V, Grinstaff MW, Snyder BD. Contrast enhanced computed tomography can predict the glycosaminoglycan content and biomechanical properties of articular cartilage. Osteoarthritis Cartilage 2010;18:184–91.
4. Frisbie DD, Al-Sobayil F, Billinghurst RC, Kawcak CE, McIlwraith CW. Changes in synovial fluid and serum biomarkers with exercise and early osteoarthritis in horses. Osteoarthritis Cartilage 2008;16:1196–204.
5. Frisbie DD, Bowman SM, Colhoun HA, DiCarlo EF, Kawcak CE, McIlwraith CW. Evaluation of autologous chondrocyte transplantation via a collagen membrane in equine articular defects – results at 12 and 18 months. Osteoarthritis Cartilage 2008;16:667–79.
6. Strickland CD, Kijowski R. Morphologic imaging of articular cartilage. Magn Reson Imag Clin N Am 2011;19:229–48.
7. Taylor C, Carballido-Gamio J, Majumdar S, Li X. Comparison of quantitative imaging of cartilage for osteoarthritis: T2, T1ρ, dGEMRIC and contrast-enhanced computed tomography. Magn Reson Imag 2009;27:779–84.
8. Nelson BB, Kawcak CE, Goodrich LR, Werpy NM, Valdés-Martínez A, McIlwraith CW. Comparison between computed tomographic arthrography, radiography, ultrasonography, and arthroscopy for the diagnosis of femorotibial joint disease in western performance horses. Vet Radiol Ultrasound 2016;57:387–402.
9. Joshi NS, Bansal PN, Stewart RC, Snyder BD, Grinstaff MW. Effect of contrast agent charge on visualization of articular cartilage using computed tomography: exploiting electrostatic interactions for improved sensitivity. J Am Chem Soc 2009;131:13234–5.
10. Bansal PN, Joshi NS, Entezari V, Malone BC, Stewart RC, Snyder BD, *et al*. Cationic contrast agents improve quantification of glycosaminoglycan (GAG) content by contrast enhanced CT imaging of cartilage. J Orthop Res 2011;29:704–9.
11. Lakin BA, Ellis DJ, Shelofsky JS, Freedman JD, Grinstaff MW, Snyder BD. Contrast-enhanced CT facilitates rapid, nondestructive assessment of cartilage and bone properties of the human metacarpal. Osteoarthritis Cartilage 2015;23:2158–66.
12. Lakin BA, Grasso DJ, Shah SS, Stewart RC, Bansal PN, Freedman JD, *et al*. Cationic agent contrast-enhanced computed tomography imaging of cartilage correlates with the compressive modulus and coefficient of friction. Osteoarthritis Cartilage 2013;21:60–8.
13. Stewart RC, Bansal PN, Entezari V, Lusic H, Nazarian RM, Snyder BD, *et al*. Contrast-enhanced CT with a high-affinity cationic contrast agent for imaging ex vivo bovine, intact ex vivo rabbit and in vivo rabbit cartilage. Radiology 2013;266:141–50.
14. Stewart RC, Patwa AN, Lusic H, Freedman JD, Wathier M, Snyder BD, *et al*. Synthesis and preclinical characterization of a cationic iodinated imaging contrast agent (CA4+) and its use for quantitative computed tomography of ex vivo human hip cartilage. J Med Chem 2017;60:5543–55.
15. Nelson BB, Stewart RC, Kawcak CE, Freedman JD, Patwa AN, Snyder BD, *et al*. Quantitative evaluation of equine articular cartilage using cationic contrast-enhanced computed tomography. Cartilage Early View 2018, https://doi.org/10.1177/1947603518812562.
16. Mashiatulla M, Moran MM, Chan D, Li J, Freedman JD, Snyder BD, *et al*. Murine articular cartilage morphology and compositional quantification with high resolution cationic contrast-enhanced muCT. J Orthop Res 2017;35:2740–8.
17. Nickmanesh R, Stewart RC, Snyder BD, Grinstaff MW, Masri BA, Wilson DR. Contrast-enhanced computed tomography (CECT) attenuation is associated with stiffness of intact knee cartilage. J Orthop Res 2018;36:2641–7.
18. Rickey EJ, Cruz AM, Trout DR, McEwen BJ, Hurtig MB. Evaluation of experimental impact injury for inducing post-traumatic osteoarthritis in the metacarpophalangeal joints of horses. Am J Vet Res 2012;73:1540–52.
19. Bolam C, Hurtig MB, Cruz A, McEwen BJE. Characterization of experimentally induced post-traumatic osteoarthritis in the medial femorotibial joint of horses. Am J Vet Res 2006;67:433–47.
20. Changoor A, Coutu JP, Garon M, Quenneville E, Hurtig MB, Buschmann MD. Streaming potential-based arthroscopic device is sensitive to cartilage changes immediately post-impact in an equine cartilage injury model. J Biomech Eng 2011;133, 061005.
21. Edwards RB, Lu Y, Uthamanthil RK, Bogdanske JJ, Muir P, Athanasiou KA, *et al*. Comparison of mechanical debridement and radiofrequency energy on chondroplasty in an in vivo equine model of partial thickness cartilage injury. Osteoarthritis Cartilage 2007;15:169–78.
22. Nelson B. Investigation of Cationic Contrast-Enhanced Computed Tomography for the Evaluation of Equine Articular Cartilage. Clinical Sciences. Ph.D. dissertation. Fort Collins, CO: Colorado State University; 20171–255.
23. Bertone AL, Palmer JL, Jones J. Synvoial fluid cytokines and eicosanoids as markers of joint disease in horses. Vet Surg 2001;30:528–38.
24. Changoor A, Fereydoonzad L, Yaroshinsky A, Buschmann MD. Effects of refrigeration and freezing on the electromechanical and biomechanical properties of articular cartilage. J Biomech Eng 2010;132, 064502.
25. Rozen B, Brosh T, Salai M, Herman A, Dudkiewicz I. The effects of prolonged deep freezing on the biomechanical properties of osteochondral allografts. Cell Tissue Bank 2009;10:27–31.
26. Brittberg M, Winalski CS. Evaluation of cartilage injuries and repair. J Bone Jt Surg 2003;85-A:58–69.
27. Huttu MR, Puhakka J, Makela JT, Takakubo Y, Tiitu V, Saarakkala S, *et al*. Cell-tissue interactions in osteoarthritic human hip joint articular cartilage. Connect Tissue Res 2014;55:282–91.
28. June RK, Mejia KL, Barone JR, Fyhrie DP. Cartilage stress-relaxation is affected by both the charge concentration and valence of solution cations. Osteoarthritis Cartilage 2009;17:669–76.
29. Lippiello L, Hall D, Mankin HJ. Collagen synthesis in normal and osteoarthritic human cartilage. J Clin Investig 1977;59:593–600.
30. McIlwraith CW, Frisbie DD, Kawcak CE, Fuller CJ, Hurtig M, Cruz A. The OARSI histopathology initiative - recommendations for histological assessments of osteoarthritis in the horse. Osteoarthritis Cartilage 2010;18:S93–S105.

31. McIlwraith CW, Frisbie DD, Rodkey WG, Kisiday JD, Werpy NM, Kawcak CE, *et al*. Evaluation of intra-articular mesenchymal stem cells to augment healing of microfractured chondral defects. Arthroscopy 2011;27:1552–61.
32. Frisbie DD, Cross MW, McIlwraith CW. A comparative study of articular cartilage thickness in the stifle of animal species used in human pre-clinical studies compared to articular cartilage thickness in the human knee. Vet Comp Orthop Traumatol 2006;19:142–6.
33. Changoor A, Hurtig MB, Runciman RJ, Quesnel AJ, Dickey JP, Lowerison M. Mapping of donor and recipient site properties for osteochondral graft reconstruction of subchondral cystic lesions in the equine stifle joint. Equine Vet J 2006;38:330–6.
34. Bland JM, Altman DG. Calculating correlation coefficients with repeated observations: Part 1–Correlation within subjects. Br Med J 1995;310. 446-446.
35. Landis JR, Koch GG. The measurement of observer agreement for categorical data. Biometrics 1977;33:159–74.
36. Lakin BA, Patel H, Holland C, Freedman JD, Shelofsky JS, Snyder BD, *et al*. Contrast-enhanced CT using a cationic contrast agent enables non-destructive assessment of the biochemical and biomechanical properties of mouse tibial plateau cartilage. J Orthop Res 2016;34:1130–8.
37. Schmitz N, Laverty S, Kraus VB, Aigner T. Basic methods in histopathology of joint tissues. Osteoarthritis Cartilage 2010;18:S113–6.
38. Fischenich KM, Button KD, DeCamp C, Haut RC, Donahue TL. Comparison of two models of post-traumatic osteoarthritis; temporal degradation of articular cartilage and menisci. J Orthop Res 2017;35:486–95.
39. Lee CM, Kisiday JD, McIlwraith CW, Grodzinsky AJ, Frisbie DD. Development of an in vitro model of injury-induced osteoarthritis in cartilage explants from adult horses through application of single-impact compressive overload. Am J Vet Res 2013;74:40–7.
40. Barton KI, Shekarforoush M, Heard BJ, Sevick JL, Vakil P, Atarod M, *et al*. Use of pre-clinical surgically induced models to understand biomechanical and biological consequences of PTOA development. J Orthop Res 2017;35:454–65.
41. Brimmo OA, Pfeiffer F, Bozynski CC, Kuroki K, Cook C, Stoker A, *et al*. Development of a novel canine model for posttraumatic osteoarthritis of the knee. J Knee Surg 2016;29:235–41.
42. Novakofski KD, Berg LC, Bronzini I, Bonnevie ED, Poland SG, Bonassar LJ, *et al*. Joint-dependent response to impact and implications for post-traumatic osteoarthritis. Osteoarthritis Cartilage 2015;23:1130–7.
43. Haut RC, Ide TM, De Camp CE. Mechanical responses of the rabbit patello-femoral joint to blunt impact. J Biomech Eng 1995;117:402–8.
44. D'Lima DD, Hashimoto S, Chen PC, Colwell Jr CW, Lotz MK. Impact of mechanical trauma on matrix and cells. Clin Orthop Relat Res 2001:S90–9.
45. Thompson Jr RC, Oegema Jr TR, Lewis JL, Wallace L. Osteoarthrotic changes after acute transarticular load. An animal model. J Bone Joint Surg Am 1991;73:990–1001.
46. Newberry WN, Zukosky DK, Haut RC. Subfracture insult to a knee joint causes alterations in the bone and in the functional stiffness of overlying cartilage. J Orthop Res 1997;15:450–5.
47. Pawson DJ, Glanzmann M, Luechinger R, Müller R, Stok KS. Quantitative morphometric patterns in cartilage and bone from the humeral heads of end-stage osteoarthritis patients. Osteoarthritis Cartilage 2015;23:1377–87.
48. Maerz T, Kurdziel M, Newton MD, Altman P, Anderson K, Matthew HW, *et al*. Subchondral and epiphyseal bone remodeling following surgical transection and noninvasive rupture of the anterior cruciate ligament as models of post-traumatic osteoarthritis. Osteoarthritis Cartilage 2016;24:698–708.
49. Li G, Yin J, Gao J, Cheng TS, Pavlos NJ, Zhang C, *et al*. Subchondral bone in osteoarthritis: insight into risk factors and microstructural changes. Arthritis Res Ther 2013;15:223.
50. Bansal PN, Stewart RC, Entezari V, Snyder BD, Grinstaff MW. Contrast agent electrostatic attraction rather than repulsion to glycosaminoglycans affords a greater contrast uptake ratio and improved quantitative CT imaging in cartilage. Osteoarthritis Cartilage 2011;19:970–6.